Neutron scattering measurements of the phonon density of states of FeSe$_{1-x}$ superconductors

D. Phelan,[1] J. N. Millican,[1] E. L. Thomas,[2] J. B. Leão,[1] Y. Qiu,[1,3] and R. Paul[1]

[1]*NIST Center for Neutron Research, National Institute of Standards and Technology, Gaithersburg, Maryland 20899, USA*
[2]*Ceramics Division, National Institute of Standards and Technology, Gaithersburg, Maryland 20899, USA*
[3]*Department of Materials Science and Engineering, University of Maryland, College Park, Maryland 20742, USA*

Inelastic neutron-scattering experiments have been carried out on polycrystalline samples of the FeSe$_{1-x}$ superconductors. We report the phonon density of states for FeSe$_{1-x}$ with $T_c \approx 8$ K. The phonon cutoff frequency is observed around 40 meV. No significant change is observed across the superconducting transition. The measurements support the published first-principles calculations [A. Subedi *et al.*, Phys. Rev. B **78**, 134514 (2008)].

I. INTRODUCTION

Recently, the family of Fe superconductors, which had consisted of only compounds containing both Fe and As, has been expanded to include Fe(Se/Te)$_{1-x}$.[1] A T_c of approximately 8 K has been reported for FeSe$_{1-x}$ at ambient pressure,[1] while a T_c of 15 K has been reported in Fe(Se$_{0.5}$Te$_{0.5}$)$_{1-x}$.[2,3] Interestingly, T_c is very sensitive to pressure and increases to 27 K by the application of 1.48 GPa in FeSe.[4] The planar features of the crystal structure of Fe(Se/Te)$_{1-x}$, which is PbO type, are similar to those of the FeAs compounds. Moreover, first-principles calculations of the band structure[5] of FeSe show analogous features in the Fermi surface to LaOFeAs. This suggests that the class of Fe(Se/Te)$_{1-x}$ materials may play an important role in elucidating the nature of the superconductivity of FeAs-based superconductors.

While the mechanism of superconductivity in Fe(Se/Te)$_{1-x}$ compounds is yet unknown, the field is developing quickly. Initially it was believed that a nonstoichiometric ratio (i.e., not 1:1) of Fe:Se was critical for the superconductivity[1] and that this nonstoichiometry resulted in anion vacancies, which could have the effect of stabilizing magnetic clusters.[6] Very recently a report has appeared that suggests that for the Te-free compounds superconductivity only appears in a narrow compositional range near perfectly stoichiometric FeSe.[7] No coherence peak, which would be typical for a phonon-mediated *s*-wave superconductor, is observed in NMR measurements.[8] A possible alternative to a phonon-mediated mechanism is an unconventional magnetic mechanism related to robust incommensurate spin correlations.[9]

In this paper, we report the results of inelastic neutron-scattering measurements performed on powder samples of FeSe$_{1-x}$, which were made to determine the phonon density of states (PDOS) at several temperatures. The PDOS is an important quantity for superconducting compounds because, according to standard electron-phonon coupling theory, T_c is related to the spectral weight of phonon vibrations. Moreover, it is a quantity that can be directly compared to theoretical calculations, and we show that there is a fair agreement between the first-principles calculations of Subedi *et al.*[5] and the current measurements.

II. EXPERIMENT

Polycrystalline FeSe$_{1-x}$ samples were synthesized by solid-state reaction from elemental Fe and Se powders. All handling was performed in an inert He glove box in which a very low humidity level (less than 35 ppm) was maintained so that, once the synthesis began, the samples measured in the inelastic neutron-scattering experiments were never exposed to the atmosphere. Initially, the desired quantities of Fe and Se were ground together and then put in a domed quartz tube connected to a closed valve. The tube was then placed in a tube furnace and heated to 110 °C with the valve opened to evacuate for an hour in order to remove any gas or moisture. The valve was then closed to minimize deposition of Se on the cold end of the tube and in the vacuum line, and the sample was heated to 670 °C for 13 h in vacuum and then cooled back down to room temperature. The sample was reground, placed back in the tube, and a similar process was carried out, except that this time, the sample was heated to 670 °C for 24 h and then the temperature was lowered to 400 °C, which was maintained for 36 h. The last step was critical for avoiding the NiAs phase of FeSe.

The motivation for handling the powders for the inelastic neutron-scattering measurements in an inert environment was to avoid hydrogen contamination in the samples due to contact with air or moisture from the air. Hydrogen contamination is undesirable for inelastic neutron-scattering measurements due to the large incoherent-scattering cross section of hydrogen. To determine the hydrogen content in the samples, sample B (see below) was analyzed by prompt gamma activation analysis (PGAA), which is a nondestructive technique for determining accurate quantities of hydrogen and other elements, on beamline NG-7 at the NIST Center for Neutron Research (NCNR).[10,11] Samples that had been handled in air exhibited a Fe/H molar ratio of approximately ten; however, the sample grown in the glove box had a significantly improved ratio of approximately 28. Relative 1σ uncertainties for the latter PGAA measurements were <10%, based on counting statistics.

Using the procedure outlined above, two samples were grown: one (sample A) with an initial Fe:Se ratio of 1.0:0.72 and the other (sample B) with a ratio of 1.0:0.82. Approximately 14 g of sample A and 12 g of sample B were sealed in
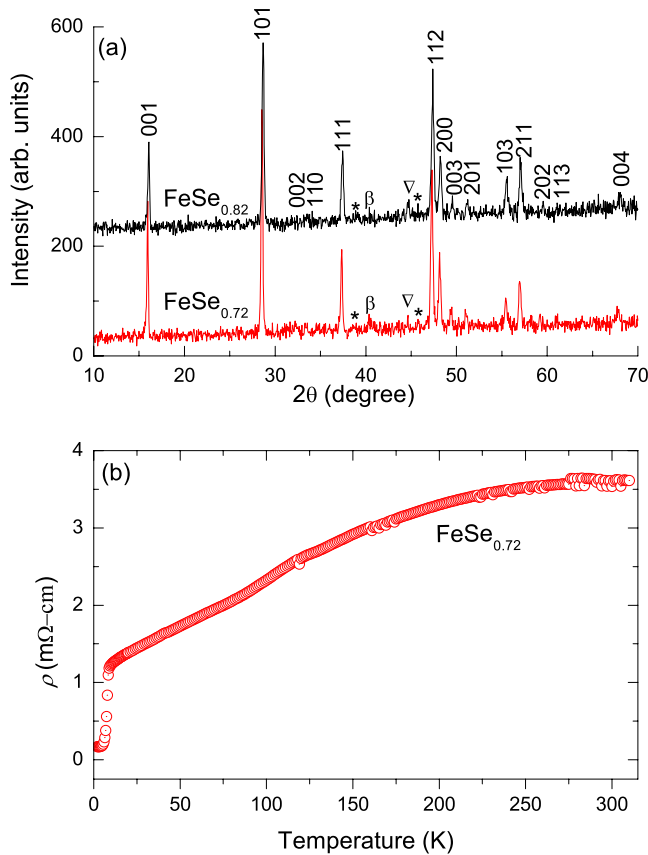
FIG. 1. (Color online) (a) X-ray diffraction patterns of samples A and B. Reflections are labeled in tetragonal ($P4/nmm$) notation. Positions of possible impurity peaks (very weak) are denoted with the symbols β, $*$, and ∇, for β-FeSe, Fe_3O_4, and Fe_3Si/Fe, respectively. (b) Electrical resistivity of sample B.

FIG. 2. (Color online) Observed (red +) and fitted (solid green) powder neutron-diffraction pattern of sample B as measured on BT-1 at (a) $T=298$ K and (b) $T=4$ K. The regions of missing data are masked and correspond to aluminum reflections. The difference curve is shown at the bottom in solid black and the calculated positions of the reflections are shown. The insets show the clear splitting of reflections at 6 K and indicate the lower symmetry of the low-temperature phase. The inclusion of a weak NiAs phase of FeSe was included to slightly improve the fits.

aluminum cans with indium gaskets while in the glove box for the inelastic neutron-scattering experiments. A remaining small quantity of both samples was also removed from the glove box for x-ray diffraction measurements and an electrical resistivity measurement. X-ray diffraction measurements were made using a commercial diffractometer with Cu $K\alpha$ radiation ($\lambda=1.5405$ Å). As shown in Fig. 1(a), both samples had very clean x-ray patterns except for a few very small potential impurity peaks which are labeled. The resistivity of sample A, shown in Fig. 1(b), was measured on a pellet that had been pressed and heated at 400 °C for 12 h. The sample undergoes a superconducting transition at 8 K. Our previous measurements of a sample grown with the same initial starting materials as sample B indicated a superconducting transition at practically the same temperature.

There are three models for the sample stoichiometry of superconducting Fe(Se/Te)$_{1-x}$ samples based on Rietveld refinements of powder neutron and x-ray diffraction data. In one model,[12] there are vacancies on anion sites. According to Refs. 9 and 13, anion sites are fully occupied and additional Fe atoms occupy interstitial sites in nonstoichiometric mixed Se/Te compositions. Finally, according to Ref. 7, superconducting Te-free samples are actually nearly stoichiometric, and the additional Fe used in the synthesis process actually forms impurities that are difficult to detect by x ray. Given
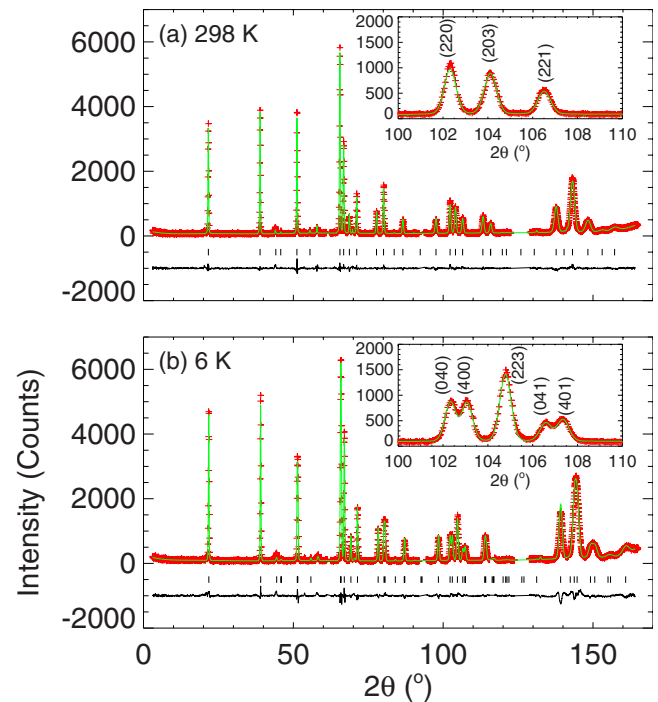
these differing results, we performed powder neutron-diffraction measurements and carried out Rietveld refinement on our samples in order to determine their stoichiometry. Powder neutron-diffraction measurements were performed on sample B on the BT-1 powder diffractometer at the NCNR with $\lambda=2.0782$ Å obtained from a Ge(311) monochromator, and Rietveld refinement was carried out using GSAS (Ref. 14) with EXPGUI interface.[15] The refinement of sample B at 298 K in tetragonal ($P4/nmms$ space group) is shown in Fig. 2(a), where it is clear that there is a very good agreement between the observed and calculated intensities, and the fitted parameters are listed in Table I. Consistent with the report of Ref. 7, we found that our sample was nearly stoichiometric. Again, consistent with Ref. 7, the placement of Fe on interstitial sites worsened the fit. The measurement at 4 K indicated that a structural phase transition had occurred, and the lower temperature phase was identified as orthorhombic (space group $Cmme$), consistent with the report of Ref. 12. The Rietveld refined pattern is shown in Fig. 2(b), and the refined positions are listed in Table I. Our data indicates that the structural phase-transition temperature was between 60 and 80 K, which is again consistent with Ref. 12. Additionally, Rietveld refinement was carried out on sample A at 300 K using the diffraction data measured on the disk chopper spectrometer (DCS) at the NCNR with $\lambda=1.8$ Å (more details of the DCS measurement are provided below).

TABLE I. Rietveld refinement results for sample B as measured on BT-1.

$T=298$ K, $P4/nmms$						
$\chi^2=1.84$, $R_{Wp}=6.73\%$, $R_p=5.37\%$						
$a=3.7724(1)$ Å, $c=5.5217(1)$ Å						
Atom	site	x	y	z	$U_{ISO}(10^{-2}$ Å$^2)$	Occ.
Fe	$2a$	0	0	0	1.14(5)	1
Se	$2c$	0	$\frac{1}{2}$	0.2673(2)	1.27(6)	1.0030(5)
$T=6$ K, $Cmme$						
$\chi^2=3.34$, $R_{Wp}=8.19\%$, $R_p=6.34\%$						
$a=5.3081(1)$ Å, $b=5.3354(1)$ Å, $c=5.4879(1)$ Å						
Atom	site	x	y	z	$U_{ISO}(10^{-2}$ Å$^2)$	Occ
Fe	$4a$	$\frac{1}{4}$	0	0	0.27(3)	1
Se	$4g$	0	$\frac{1}{4}$	0.7352(2)	0.25(6)	0.988(6)

Similarly, the best refinement showed the sample was nearly stoichiometric (the best fit was FeSe$_{.99}$). As it appears that samples A and B have essentially the same stoichiometry, it is clear that sample A has a larger content of Fe-based impurities, such as Fe, Fe$_3$O$_4$, and Fe$_3$Si than sample B. As pointed out in Ref. 7, such impurities are not easily detected by x-ray diffraction but are much easier to see by neutron diffraction, which explains why the x-ray patterns in Fig. 1 are clean. The overlap of Fe and Al Bragg reflections in our neutron-scattering experiments makes it impossible to determine the precise phase fractions of Fe or Fe$_3$Si in the sample but, since the refinement of occupancies in FeSe strongly indicates the sample is nearly stoichiometric, it can be inferred that the additional Fe atoms form impurities. As discussed in the following section, a comparison of the inelastic spectra of samples A and B gives an indication that the scattering from such impurities in the PDOS is not substantial.

Inelastic neutron-scattering measurements were made on the BT-4 filter-analyzer spectrometer (FANS) at the NCNR. The operational principle of the measurement is described in Ref. 16. A pyrolitic graphite (PG) (002) monochromator was used for measurements of energy transfer, $\hbar\omega=E_i-E_f$ (where E_i and E_f are the incident and scattered-neutron energies, respectively), from 5 to 44 meV with collimations of 40′-40′ (in pile—post monochromator), giving an energy resolution that varied from 1.1 meV full width at half maximum (FWHM) at $\hbar\omega=5$–3.9 meV at $\hbar\omega=44$ meV. A Cu(220) monochromator was used for measurements with $\hbar\omega$ from 35 to 107 meV with collimations of 40′-40′, giving an energy resolution that varied from 1.5 meV FWHM at $\hbar\omega=44$–5 meV at $\hbar\omega=107$ meV. The sample was measured while in a top-loading closed cycle refrigerator with a base temperature of 3.8 K. Cadmium masks covered both the top and bottom flanges of the aluminum can to minimize the background. The inelastic measurements were repeated on an identical empty sample can to determine the background.

Additional inelastic neutron-scattering measurements at lower values of $\hbar\omega$ were performed on DCS at the NCNR.[17] Measurements were made with incident wavelengths of 1.8, 2.9, 4.8, and 7.0 Å although all the data shown here were

taken with $\lambda=1.8$ Å. The sample was measured in a He cryostat with a base temperature of 1.5 K in the same aluminum sample can used for FANS. The DAVE software package was used for elements of the data reduction and analysis.[18]

III. RESULTS AND DISCUSSION

For a measurement on FANS, the scattered-neutron energy is chosen by a series of filters that only allow neutrons in a narrow band with $\langle E_f \rangle=1.2$ meV to pass through.[19] After subtracting out the background, the measured intensity, $I(\omega)$ is approximately proportional to the neutron-weighted PDOS,[16] $G(\omega)$, given by[20]

$$G(\omega) = \sum_i \sigma_i \exp(-2W_i)G_i(\omega)/m_i, \qquad (1)$$

where the sum occurs over the different atomic species—in this case, Fe and Se. σ_i, m_i, and W_i are the neutron-scattering cross section, the atomic mass, and the Debye-Waller factor for atom species i. The incoherent approximation is made so that the σ_i are the total (sum of incoherent and coherent) cross sections, which are 11.62 and 8.30 b for Fe and Se, respectively. Thus, the $\frac{\sigma}{m}$ weighting is 1.98–1 for Fe to Se. $G_i(\omega)$ is the partial weighted PDOS defined by

$$G_i(\omega) = \frac{1}{3N}\sum_{j,\vec{k}} |\vec{e}_i(j,\vec{k})|^2 \delta[\omega - \omega(j,\vec{k})], \qquad (2)$$

where the sum occurs over all phonon modes, j, and wave vectors $\vec{k}$, and the eigenvector and frequency of a given mode are denoted by $\vec{e}_i(j,\vec{k})$ and $\omega(j,\vec{k})$.

The observed PDOS of sample A at 3.8 K as measured on FANS is shown in Fig. 3(a). The measurement of the empty can has been subtracted out as background. The phonons have a well-defined cutoff frequency of approximately 41 meV. Between 10 and 40 meV, six distinct peaks in the density of states are observed at 12, 17.5, 20.5, 24.5, 31.5, and 38 meV. Note that the three peaks below 10 meV are not reliable because the scattering at those energies suffers from
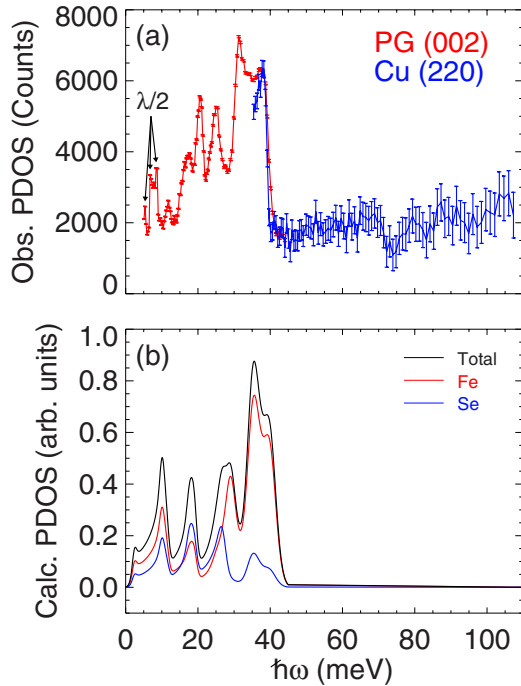
FIG. 3. (Color online) (a) The measured PDOS of sample A at 3.8 K. Data taken with the PG (002) monochromator is shown in red, whereas data taken with the Cu (220) monochromator is shown in blue. The empty can background has been subtracted from both measurements. The Cu data is multiplied by a constant term to put the same data on the scale with the PG data. The reason that there is a larger dip in the Cu intensity than the PG intensity around 35 meV is that the energy resolution of the Cu monochromator is superior at that energy transfer to that of the PG monochromator. The three peaks below 10 meV are marked for their $\frac{\lambda}{2}$ contamination. (b) The partial PDOS of Fe and Se and the total PDOS, as described in the text. The error bars in (a) and later figures represent the $\pm 1\sigma$ statistical uncertainty.

$\frac{\lambda}{2}$ contamination from the three highest peaks in the PDOS.[21]

Since reliable data could not be collected below 10 meV on FANS, an additional measurement of the low-energy phonons was made on DCS with an incident wavelength of 1.8 Å for sample A. The background was subtracted out as determined by the intensity at high energy transfers ($E_i < E_f$) at 1.5 K, where no inelastic scattering is expected. Figure 4(a) shows the Q-integrated intensity, $I(\hbar\omega) = \int_{1.5\ \text{Å}^{-1}}^{6.5} I(Q,\hbar\omega)dQ$, at $T = 1.5$, 100, 200, and 300 K. Two peaks are evident at 300 K: one at 8.5 meV and the other at 5.5 meV. As the temperature is lowered, the intensity corresponding to both peaks decreases due to a reduced thermal population of phonons, and the peak at 5.5 meV becomes too weak to resolve at 1.5 K. The peak at 8.5 meV continually hardens, shifting to ≈ 9.3 meV, as the temperature is lowered to 1.5 K. The peaks in the PDOS above 10 meV are difficult to observe using DCS. This is because measured phonon intensity decreases as the inverse of $\hbar\omega$ and the flux of neutrons on DCS is much weaker than that of FANS. Although there is an observed peak at $\hbar\omega = 17$ meV, there is also a known detector spurion for DCS there so it is much more reliable to trust the data for $\hbar\omega > 10$ meV on FANS. Figure 4(b) shows the energy-integrated intensity, $I(Q)$

$= \int_{-11\ \text{meV}}^{-3} I(Q,\hbar\omega)d\hbar\omega$, also at $T = 1.5$, 100, 200, and 300 K. Figure 4(b) also shows a scaled down $I(Q,\hbar\omega=0)$. Since for inelastic scattering from phonons, $I(Q)$ is approximately proportional to $Q^2 I(Q,\hbar\omega=0)$,[22] this shows that the inelastic scattering over this energy range is indeed from phonons.

The PDOS of sample A was measured below (3.8 K) and above (13 K) T_c on FANS, as shown in Fig. 5. No clear difference in the PDOS could be detected across the superconducting transition given the experimental statistics. A similar lack of change of the PDOS was reported for LaFeOAs.[23] The PDOS of sample B is also shown in Fig. 5 at 3.8 and 100 K. The similarity of the measurements of samples A and B at 3.8 K indicates that the inelastic scattering from Fe-based impurities is minimal since sample A has a higher impurity content than sample B. The comparison between 3.8 (orthorhombic) and 100 K (tetragonal) data shows that the spectral weight of the phonons is relatively unaffected by the structural phase transition.

The bare PDOS according to the calculation of Subedi *et al.*[5] for stoichiometric FeSe is shown in Fig. 3(b) along with the bare partial PDOS of Fe and Se. The calculation has been convoluted with the instrumental resolution function of FANS with the PG monochromator and the PDOS of Fe and Se have been weighted by $\frac{\sigma_i}{m_i}$. It should be noted that the bare PDOS and the neutron-weighted PDOS are different in that the neutron-weighted PDOS is weighted by the squared moduli of eigenvectors, which will cause a small difference in the observed peak heights of the two quantities since Fe and Se have difference atomic masses, but the peak positions are expected not to be very sensitive to this difference.[22,24] According to the calculation, there are four main bands of phonons. The highest energy band is predicted to be a doublet, as we observe, with peaks at 39 meV, which is close to the observed value, and 36 meV, which is 4–5 meV higher than the observed value. The second highest band is centered at 28 meV, which we also observe at 24.5 meV. The third highest band is at 18 meV; we observe a split band with peaks at 17.5 and 20.5 meV although the calculation shows that there should be a shoulder at the lower energy transfer so the observed splitting is not unreasonable. The same bare PDOS calculation is also shown in Fig. 4(c) for the lower energy phonons. The calculation has been corrected for the Bose factor and the $\frac{1}{\hbar\omega}$ term in the scattering cross section for phonons,[22] and also convoluted with the instrument resolution function so that it can be compared more directly with observed spectra. All temperature dependence emanates from the Bose factor (the same bare PDOS is used for all temperatures.) The agreement between the observed and predicted peaks is quite good at 1.5 K where the calculation is most apt. The calculation predicts a peak around 10 meV, which is consistent with the experiment—within 1 meV at 1.5 K. The main difference between the calculation and the measurement is that a peak is observed at 5 meV at higher temperatures, whereas the calculation predicts the peak between 2 and 3 meV. Thus all bands of phonons predicted by the calculation are observed in the experiment with only small differences in individual peaks.

The main conclusion of the phonon calculations is that standard electron-phonon coupling cannot account for a T_c of
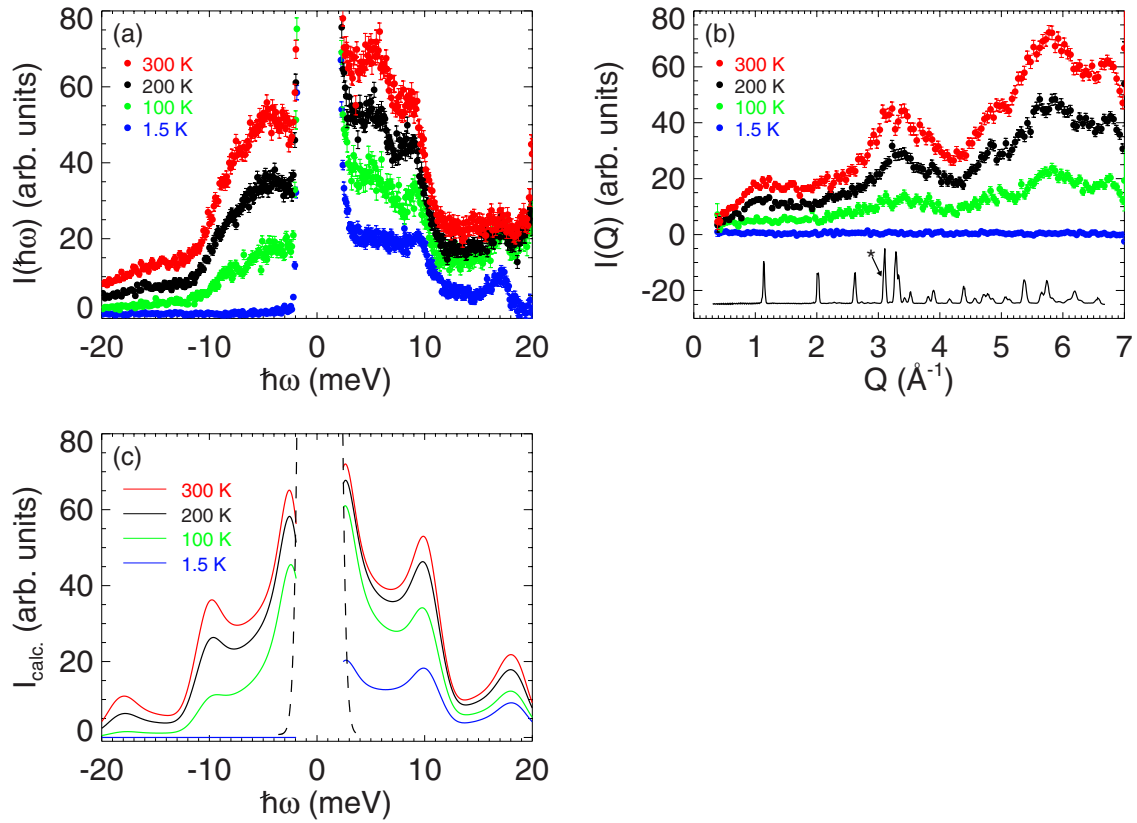
FIG. 4. (Color online) (a) $I(\hbar\omega)$, in (a), and $I(q)$, in (b), for sample A at $T=1.5$, 100, 200, and 300 K. $I(Q,\hbar\omega=0)$, i.e., the diffraction pattern, has been scaled down and is shown at the bottom. The particularly strong Bragg reflection at $Q=3.1$ Å^{-1} is marked with an asterisk for its contamination from the Al sample can and also Fe/Fe$_3$Si impurities. (c) The expected inelastic-scattering spectrum based on the PDOS calculation.

even 1 K. The closeness of the observed and calculated phonon cutoff frequencies along with the observation of all predicted modes with only small shifts in energy support this conclusion. We note that similar electron-phonon calculations and subsequent neutron measurements find the same conclusion for LaFeAsO.[23,24] On the other hand, PDOS measurements and electron-phonon coupling calculations agree in explaining the superconductivity in other systems such as MgB$_2$.[22,25]

Finally, we note that recently a magnetic resonance has been observed by inelastic neutron-scattering measurements of a powder sample of Ba$_{0.6}$K$_{0.4}$Fe$_2$As$_2$,[26] a result that suggests that spin fluctuations in the superconducting state could be a universal feature of cuprate, heavy fermion, and iron superconductors. If the resonant energy, $\hbar\omega_r$, scales as 4.2 times that of T_c as observed in that Ba$_{0.6}$K$_{0.4}$Fe$_2$As$_2$, then $\hbar\omega_r$ should be approximately 2.9 meV for FeSe. We could not observe any magnetic resonance in our experiments on DCS, which is similar to the findings for LaO$_{0.87}$F$_{0.13}$FeAs made on the same instrument.[24]

IV. CONCLUSION

In conclusion, we used inelastic neutron-scattering techniques in investigating the FeSe$_{1-x}$ superconductors. We did not observe a significant change in the PDOS across the su-

perconducting transition temperature nor did we observe a large change across the orthorhombic-tetragonal phase transition. Our results are in general support of the calculations of Subedi *et al.*,[5] which suggests that their calculation of electron-phonon coupling is reasonable.
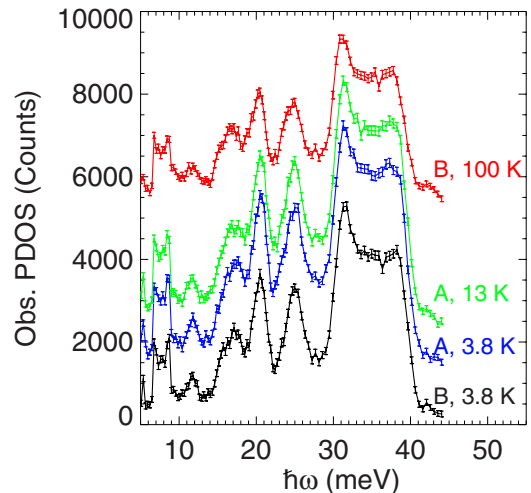

FIG. 5. (Color online) A comparison of the measured PDOS of sample A at 3.8 and 13 K and sample B at 3.8 and 100 K. Data are intentionally offset for clarity.

[1] F.-C. Hsu *et al.*, Proc. Natl. Acad. Sci. U.S.A. **105**, 14262 (2008).

[2] K.-W. Yeh, T.-W. Huang, Y.-L. Huang, T.-K. Chen, F.-C. Hsu, P. M. Wu, Y.-C. Lee, Y.-Y. Chu, C.-L. Chen, J.-Y. Luo, D.-C. Yan, and M.-K. Wu, Europhys. Lett. **84**, 37002 (2008).

[3] M. Fang, H. Pham, B. Qian, T. Liu, E. Vehstedt, Y. Liu, L. Spinu, and Z. Mao, Phys. Rev. B **78**, 224503 (2008).

[4] Y. Mizuguchi, F. Tomioka, S. Tsuda, T. Yamaguchi, and Y. Takano, Appl. Phys. Lett. **93**, 152505 (2008).

[5] A. Subedi, L. Zhang, D. J. Singh, and M. H. Du, Phys. Rev. B **78**, 134514 (2008).

[6] K.-W. Lee, V. Pardo, and W. E. Pickett, Phys. Rev. B **78**, 174502 (2008).

[7] T. M. McQueen, Q. Huang, V. Ksenofontov, C. Felser, Q. Xu, H. W. Zandbergen, Y. S. Hor, J. Allred, A. J. Williams, D. Qu, J. Checkelsky, N. P. Ong, and R. J. Cava, arXiv:0811.1613, Phys. Rev. B (to be published).

[8] H. Kotegawa, S. Masaki, Y. Awai, H. Tou, Y. Mizuguchi, and Y. Takano, J. Phys. Soc. Jpn. **77**, 113703 (2008).

[9] W. Bao, Y. Qiu, Q. Huang, M. A. Green, P. Zajdel, M. R. Fitzsimmons, M. Zhemenkov, M. Fang, B. Qian, E. K. Vehstedt, J. Yang, H. M. Pham, L. Spinu, and Z. Q. Mao, arXiv:0809.2058 (unpublished).

[10] R. Paul, R. Lindstrom, and A. Heald, J. Radioanal. Nucl. Chem. **215**, 63 (1997).

[11] R. Paul, Analyst (Cambridge, U.K.) **122**, 35(R) (1997).

[12] S. Margadonna, Y. Takabayashi, M. McDonald, K. Kasperkiewicz, Y. Mizuguchi, Y. Takano, A. Fitch, E. Suarde, and K. Prassides, Chem. Commun. (Cambridge) 2008, 5607.

[13] Shiliang Li, Clarina de la Cruz, Q. Huang, Y. Chen, J. W. Lynn, Jiangping Hu, Yi-Lin Huang, Fong-chi Hsu, Kuo-Wei Yeh, Maw-Kuen Wu, and Pengcheng Dai, arXiv:0811.0195, Phys. Rev. B (to be published).

[14] A. C. Larson and R. B. V. Dreele, Los Alamos National Laboratory Report: LAUR 86–748, 2004 (unpublished).

[15] B. H. Toby, J. Appl. Crystallogr. **34**, 210 (2001).

[16] J. Copley, D. Neumann, and W. Kamitakahara, Can. J. Phys. **73**, 763 (1995).

[17] J. Copley and J. Cook, Chem. Phys. **292**, 477 (2003).

[18] http://www.ncnr.nist.gov/dave

[19] T. Udovic *et al.*, Nucl. Instrum. Methods Phys. Res. A **588**, 406 (2008).

[20] Here $G(\omega)$ is defined consistent with the generalized density of states (GDOS) in Ref. 22. Note that the well-known $\frac{Q^2}{\omega}$ term in the formula for observed inelastic neutron-scattering intensity from phonons is cancelled out by the trajectory of $Q-\omega$ space probed by FANS as discussed in Ref. 16.

[21] The half-lambda contamination is the result of the second-order Bragg reflection of incident neutrons through the monochromator that have half the wavelength and thus four times the incident energy as the principally reflected neutrons. This leads to peaks that appear in the measurement at the energy transfer $\hbar\omega$ but actually result from the features that have a real energy transfer of $4\hbar\omega+3.6$ meV.

[22] R. Osborn, E. A. Goremychkin, A. I. Kolesnikov, and D. G. Hinks, Phys. Rev. Lett. **87**, 017005 (2001).

[23] A. Christianson *et al.*, Phys. Rev. Lett. **101**, 157004 (2008).

[24] Y. Qiu *et al.*, Phys. Rev. B **78**, 052508 (2008).

[25] T. Yildirim *et al.*, Phys. Rev. Lett. **87**, 037001 (2001).

[26] A. D. Christianson, E. A. Goremychkin, R. Osborn, S. Rosenkranz, M. D. Lumsden, C. D. Malliakas, I. S. Todorov, H. Claus, D. Y. Chung, M. G. Kanatzidis, R. I. Bewley, and T. Guidi, Nature (London) **456**, 930 (2008).